

First Observation of the $\Lambda(1405)$ Line Shape in Electroproduction

H.Y. Lu,^{1,*} R.A. Schumacher,^{1,†} K.P. Adhikari,²⁹ D. Adikaram,²⁹ M. Aghasyan,¹⁸ M.J. Amarian,²⁹ S. Anefalos Pereira,¹⁸ J. Ball,⁷ M. Battaglieri,¹⁹ V. Batourine,³⁵ I. Bedlinskiy,²² A.S. Biselli,^{11,1} S. Boiarinov,³⁵ W.J. Briscoe,¹⁵ W.K. Brooks,^{36,35} V.D. Burkert,³⁵ D.S. Carman,³⁵ A. Celentano,¹⁹ S. Chandavar,²⁸ P.L. Cole,^{16,35} P. Collins,⁶ M. Contalbrigo,¹⁷ O. Cortes,¹⁶ V. Crede,¹³ A. D'Angelo,^{20,32} N. Dashyan,⁴⁰ R. De Vita,¹⁹ E. De Sanctis,¹⁸ A. Deur,³⁵ C. Djalali,³⁴ D. Doughty,^{8,35} R. Dupre,²¹ H. Egiyan,³⁵ A. El Alaoui,² L. El Fassi,² P. Eugenio,¹³ G. Fedotov,^{34,33} S. Fegan,¹⁹ J.A. Fleming,¹⁰ M. Gabrielyan,¹² N. Gevorgyan,⁴⁰ G.P. Gilfoyle,³¹ K.L. Giovanetti,²³ F.X. Girod,³⁵ J.T. Goetz,²⁸ W. Gohn,⁹ E. Golovatch,³³ R.W. Gothe,³⁴ K.A. Griffioen,³⁹ M. Guidal,²¹ L. Guo,^{12,35} K. Hafidi,² H. Hakobyan,^{36,40} N. Harrison,⁹ D. Heddle,^{8,35} K. Hicks,²⁸ D. Ho,¹ M. Holtrop,²⁶ C.E. Hyde,²⁹ Y. Ilieva,^{34,15} D.G. Ireland,³⁷ B.S. Ishkhanov,³³ E.L. Isupov,³³ H.S. Jo,²¹ D. Keller,³⁸ M. Khandaker,²⁷ W. Kim,²⁴ A. Klein,²⁹ F.J. Klein,⁶ S. Koirala,²⁹ A. Kubarovskiy,^{9,33} V. Kubarovskiy,^{35,30} S.V. Kuleshov,^{36,22} S. Lewis,³⁷ K. Livingston,³⁷ I.J.D. MacGregor,³⁷ D. Martinez,¹⁶ M. Mayer,²⁹ B. McKinnon,³⁷ C.A. Meyer,¹ T. Mineeva,⁹ M. Mirazita,¹⁸ V. Mokeev,^{35,33} R.A. Montgomery,³⁷ K. Moriya,^{1,‡} H. Moutarde,⁷ E. Munevar,³⁵ C. Munoz Camacho,²¹ P. Nadel-Turonski,³⁵ C.S. Nepali,²⁹ S. Niccolai,²¹ G. Niculescu,^{23,28} I. Niculescu,²³ M. Osipenko,¹⁹ A.I. Ostrovidov,¹³ L.L. Pappalardo,¹⁷ R. Paremuzyan,²¹ K. Park,^{35,24} S. Park,¹³ E. Pasyuk,^{35,3} P. Peng,³⁸ E. Phelps,³⁴ J.J. Phillips,³⁷ S. Pisano,¹⁸ O. Pogorelko,²² S. Pozdniakov,²² J.W. Price,⁴ S. Procureur,⁷ Y. Prok,^{29,38,35} D. Protopopescu,³⁷ A.J.R. Puckett,³⁵ B.A. Raue,^{12,35} D. Rimal,¹² M. Ripani,¹⁹ G. Rosner,³⁷ P. Rossi,¹⁸ F. Sabatié,⁷ M.S. Saini,¹³ C. Salgado,²⁷ D. Schott,¹⁵ E. Seder,⁹ H. Seraydaryan,²⁹ Y.G. Sharabian,³⁵ G.D. Smith,³⁷ D.I. Sober,⁶ D. Sokhan,³⁷ S.S. Stepanyan,²⁴ P. Stoler,³⁰ S. Strauch,^{34,15} M. Taiuti,¹⁴ W. Tang,²⁸ Ye Tian,³⁴ S. Tkachenko,^{38,29} B. Torayev,²⁹ B. Vernarsky,¹ H. Voskanyan,⁴⁰ E. Voutier,²⁵ N.K. Walford,⁶ D.P. Weygand,³⁵ M.H. Wood,^{5,34} N. Zachariou,³⁴ L. Zana,²⁶ J. Zhang,³⁵ and Z.W. Zhao³⁸

(CLAS Collaboration)

¹Carnegie Mellon University, Pittsburgh, Pennsylvania 15213

²Argonne National Laboratory, Argonne, Illinois 60439

³Arizona State University, Tempe, Arizona 85287-1504

⁴California State University, Dominguez Hills, Carson, CA 90747

⁵Canisius College, Buffalo, NY 14208

⁶Catholic University of America, Washington, D.C. 20064

⁷CEA, Centre de Saclay, Irfu/Service de Physique Nucléaire, 91191 Gif-sur-Yvette, France

⁸Christopher Newport University, Newport News, Virginia 23606

⁹University of Connecticut, Storrs, Connecticut 06269

¹⁰Edinburgh University, Edinburgh EH9 3JZ, United Kingdom

¹¹Fairfield University, Fairfield CT 06824

¹²Florida International University, Miami, Florida 33199

¹³Florida State University, Tallahassee, Florida 32306

¹⁴Università di Genova, 16146 Genova, Italy

¹⁵The George Washington University, Washington, DC 20052

¹⁶Idaho State University, Pocatello, Idaho 83209

¹⁷INFN, Sezione di Ferrara, 44100 Ferrara, Italy

¹⁸INFN, Laboratori Nazionali di Frascati, 00044 Frascati, Italy

¹⁹INFN, Sezione di Genova, 16146 Genova, Italy

²⁰INFN, Sezione di Roma Tor Vergata, 00133 Rome, Italy

²¹Institut de Physique Nucléaire ORSAY, Orsay, France

²²Institute of Theoretical and Experimental Physics, Moscow, 117259, Russia

²³James Madison University, Harrisonburg, Virginia 22807

²⁴Kyungpook National University, Daegu 702-701, Republic of Korea

²⁵LPSC, Université Joseph Fourier, CNRS/IN2P3, INPG, Grenoble, France

²⁶University of New Hampshire, Durham, New Hampshire 03824-3568

²⁷Norfolk State University, Norfolk, Virginia 23504

²⁸Ohio University, Athens, Ohio 45701

²⁹Old Dominion University, Norfolk, Virginia 23529

³⁰Rensselaer Polytechnic Institute, Troy, New York 12180-3590

³¹University of Richmond, Richmond, Virginia 23173

³²Università di Roma Tor Vergata, 00133 Rome Italy

³³Skobeltsyn Nuclear Physics Institute, 119899 Moscow, Russia

³⁴University of South Carolina, Columbia, South Carolina 29208

³⁵Thomas Jefferson National Accelerator Facility, Newport News, Virginia 23606

³⁶Universidad Técnica Federico Santa María, Casilla 110-V Valparaíso, Chile

³⁷University of Glasgow, Glasgow G12 8QQ, United Kingdom

³⁸University of Virginia, Charlottesville, Virginia 22901

³⁹College of William and Mary, Williamsburg, Virginia 23187-8795

⁴⁰Yerevan Physics Institute, 375036 Yerevan, Armenia

(Dated: October 31, 2018)

We report the first observation of the line shape of the $\Lambda(1405)$ from electroproduction, and show that it is not a simple Breit-Wigner resonance. Electroproduction of $K^+\Lambda(1405)$ off the proton was studied by using data from CLAS at Jefferson Lab in the range $1.0 < Q^2 < 3.0$ (GeV/c)². The analysis utilized the decay channels $\Sigma^+\pi^-$ of the $\Lambda(1405)$ and $p\pi^0$ of the Σ^+ . Neither the standard (PDG) resonance parameters, nor free parameters fitting to a single Breit-Wigner resonance represent the line shape. In our fits, the line shape corresponds approximately to predictions of a two-pole meson-baryon picture of the $\Lambda(1405)$, with a lower mass pole near 1368 MeV/c² and a higher mass pole near 1423 MeV/c². Furthermore, with increasing photon virtuality the mass distribution shifts toward the higher mass pole.

PACS numbers: 13.40.-f, 13.30.Eg, 14.20.Jn, 14.20.Gk

I. INTRODUCTION

The continued study of excited baryons is needed to refine our knowledge of QCD. Probing states with peculiar properties is of particular interest toward this goal. One such object is the $\Lambda(1405)$, which has the quantum numbers $I(J^P) = 0(\frac{1}{2}^-)$, mass $m = 1405.1$ MeV/c², and full width $\Gamma = 50$ MeV/c² according to the Particle Data Group (PDG) [1]. It was first predicted by Dalitz and Tuan [2, 3] as a quasi-bound $N\bar{K}$ state that decays to $\Sigma\pi$, and was first observed by Alston *et al.* [4] in 1961.

A quark model for the spectrum of baryons with a non-relativistic harmonic oscillator potential and spin-spin hyperfine interaction between the quarks was proposed by Isgur and Karl [5, 6, 7]. This model reproduced all the observed P -wave negative parity resonances well, except for the $\Lambda(1405)$. The mass of the $\Lambda(1405)$ was predicted around 1490 MeV/c², leaving a discrepancy of about 80 MeV/c². The model was extended to include relativistic dynamics by Capstick and Isgur [8] but this mass discrepancy remained. Following an earlier paper by Oller and Meißner [9], Jido *et al.* [10] used a chiral unitary formalism to describe the $\Lambda(1405)$ as a composite of two dynamically generated $I = 0$ poles, at $m_0^{low} = 1.390 + i0.066$ GeV/c² and $m_0^{high} = 1.420 + i0.016$ GeV/c². Hence the key conclusion of this approach is that the mass distribution, or “line shape” of the $\Lambda(1405)$ is formed by two poles in the complex energy plane instead of one resonance. The higher mass pole couples more strongly to $N\bar{K}$, while the lower mass pole couples more strongly to $\Sigma\pi$. Furthermore, the line shape is expected to depend upon which reaction channel excites it. For a recent review of the extensive literature on baryonic systems within the chiral unitary framework, see Ref. [11]. There are several other detailed predictions for the parameters that characterize the poles making up

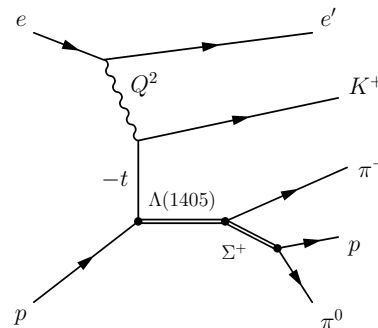


FIG. 1. The presumed primary diagram for electroproduction of the $\Lambda(1405)$ at the kinematics of the present experiment.

the $\Lambda(1405)$ mass region, for example Refs. [12–16]. One finds that theory is not in agreement about where these poles sit.

The most extensive experimental study of the $\Lambda(1405)$ mass region used real photoproduction with data from CLAS/JLab [17, 18] and also LEPS/SPring-8 [19, 20]. Support for a strongly distorted line shape was found, possibly consistent with two $I = 0$ poles, as well as evidence for interference with $I = 1$ components of the reaction mechanism. Further recent results came from pp collisions at HADES/GSI [21] and COSY/Jülich [22]. Low-statistics bubble-chamber hadronic beam data exist for K^-p [23], K^-D [24], and π^-p [25] reactions. Each case seems to show variations in the mass distribution of the $\Lambda(1405)$. To date there is no theoretical work giving any prediction for electroproduction of the $\Lambda(1405)$. The line shape seen in electroproduction could reveal features not seen in other production channels. The virtual photon exchanged in electroproduction ($Q^2 > 0$) may couple differently to the $\Lambda(1405)$ than the real photon ($Q^2 = 0$). Therefore the present study represents an exploration of an unknown corner of $\Lambda(1405)$ phenomenology.

Figure 1 shows the presumed main contribution to the $\Lambda(1405)$ electroproduction. Normally, K -nucleon scattering cannot produce this state since it lies below threshold. However, the off-shell nature of the exchanged strange meson allows the reaction to proceed. The electron scat-

* Current address: University of Iowa, Iowa City, IA 52242

† Contact: schumacher@cmu.edu

‡ Current address: Indiana University, Bloomington, Indiana 47405

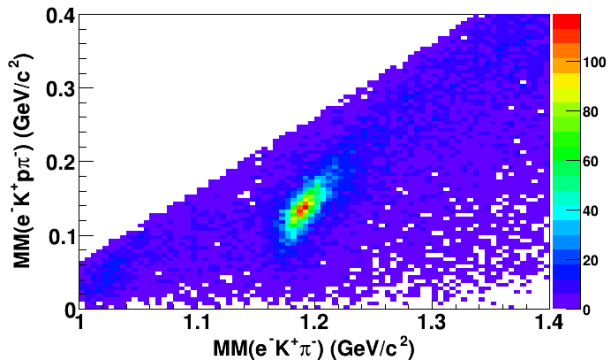


FIG. 2. (Color online) Missing mass of $e^- K^+ p \pi^-$ versus missing mass of $e^- K^+ \pi^-$ from data. The strong central peak contains the $\Sigma^+ \pi^0$ events selected for analysis.

tering process is characterized by the four-momentum transfer Q^2 , but this is one step removed from the four-momentum of the exchanged kaon, t . At our kinematics $-t$ covers the range from 0.5 to 4.5 $(\text{GeV}/c)^2$.

This work analyzed data from the “elf” run in Hall B at Jefferson Lab collected using the CLAS spectrometer [26]. It utilized a 5.5 GeV electron beam and a liquid hydrogen target. The $\Lambda(1405)$ decays solely to $\Sigma\pi$ according to the PDG [1]. The decay channel used in this analysis was $\Sigma^+ \pi^-$ for the $\Lambda(1405)$ and $p \pi^0$ for the Σ^+ . Therefore, the final detected particles were the scattered electron e^- and the K^+ , p , and π^- , while a π^0 was missing for the exclusive electroproduction of the $\Lambda(1405)$. Thus, events with exactly these four charged particles were selected.

The data analysis is described in Sec. II, followed by presentation of the results in Sec. III. The results are discussed and summarized in Sec. IV. Note that a preliminary version of this analysis was published previously [27].

II. DATA ANALYSIS

The missing mass of $e^- K^+ p \pi^-$ versus the missing mass of $e^- K^+ \pi^-$ is shown in Fig. 2. The missing π^0 's and Σ^+ 's are clearly seen near the center of Fig. 2. A selection was made by requiring the missing mass of $e^- K^+ p \pi^-$ between 0.05 and 0.25 GeV/c^2 and the missing mass of $e^- K^+ \pi^-$ to lie between 1.140 and 1.240 GeV/c^2 . The Q^2 range of significance, after the selection, was from 1.0 to 3.0 $(\text{GeV}/c)^2$. The $\Sigma^+ \pi^-$ hyperon mass spectrum that results from computing the missing mass from the $e^- K^+$ pair is shown in Fig. 3. Two ranges of Q^2 are shown, from 1.0 to 1.5 $(\text{GeV}/c)^2$ in Fig. 3(a), and from 1.5 to 3.0 $(\text{GeV}/c)^2$ in Fig. 3(b). No acceptance correction or background subtraction have been made at this stage. A bump in the $\Lambda(1405)$ region and the $\Lambda(1520)$ peak are clearly visible.

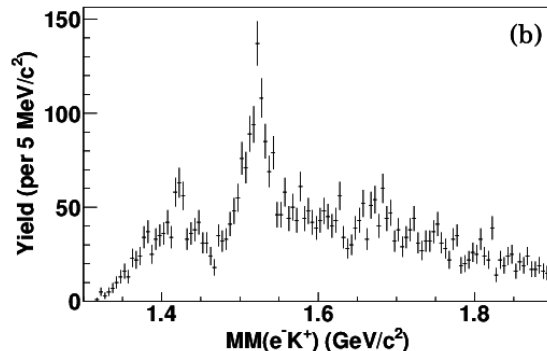
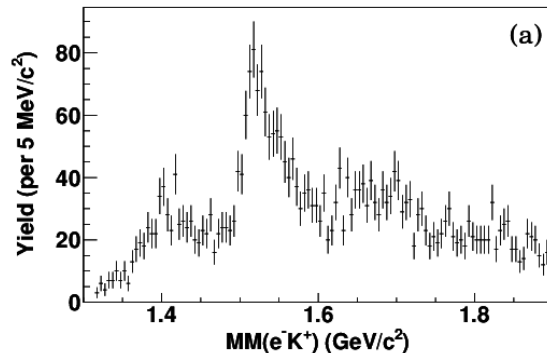


FIG. 3. Number of counts plotted versus the missing mass of $e^- K^+$ without either acceptance corrections or background subtraction for (a) $1.0 \leq Q^2 \leq 1.5$ $(\text{GeV}/c)^2$, and (b) $1.5 \leq Q^2 \leq 3.0$ $(\text{GeV}/c)^2$.

The background is mostly from non-resonant electroproduction of $K^+ \Sigma^+ \pi^-$ and resonant $K^{*0} \Sigma^+$, where the K^{*0} decays into K^+ and π^- . These background reaction channels were simulated using the CLAS standard simulation package GSIM based on GEANT [28]. Events were generated according to a phase space distribution. The invariant mass of K^+ and π^- was fitted with simulations of the two background channels. The total fit to the data set, with contributions from $K^{*0} \Sigma^+$ and $K^+ \Sigma^+ \pi^-$, is shown in Fig. 4. The K^{*0} background contribution to the combined simulated background channels was determined from this fit. This fixed ratio was used in subsequent fits to the line shapes in the hyperon mass region of interest.

A third production channel leading to the same final state particles is electroproduction of $\Sigma^{*0}(1385)$ decaying to $\Sigma^+ \pi^-$. This contamination was measured by extracting the yield of the $\Sigma^{*0}(1385)$ decaying through its dominant $\Lambda \pi^0$ channel (branching fraction 88%). This yield was rescaled to $\Sigma^+ \pi^-$ decay (6%) and modified by the computed respective acceptances. The contamination from $\Sigma^{*0}(1385)$ was thereby measured to be smaller than the statistical fluctuation in each bin and therefore negligible. The estimated yield of $\Sigma^{*0}(1385)$ and the measured yield of $\Sigma^+ \pi^-$ are shown in Fig. 5. The

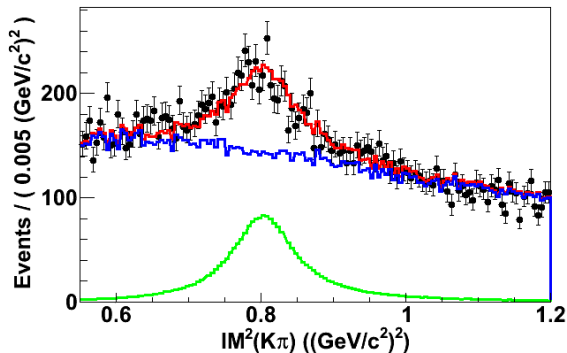


FIG. 4. (Color online) Invariant mass squared of $K^+\pi^-$. Points with error bars are measured data, the matching (red) line is the total fit to the data with two background simulations. The (green) line at the bottom is the simulation of $K^{*0}\Sigma^+$, and the upper (blue) line is simulation of $K^+\Sigma^+\pi^-$.

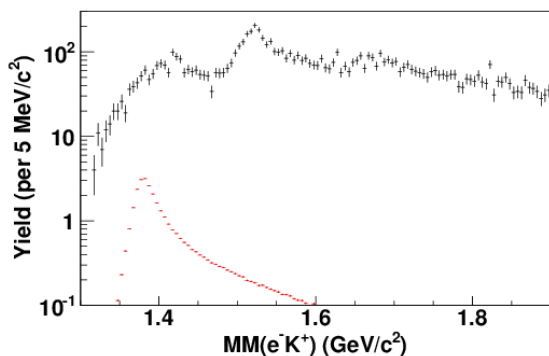


FIG. 5. (Color online) Estimated rescaled yield of the Σ^{*0} contamination shown in red (lower points) and missing mass of e^-K^+ in black (upper points). The upper points are the sum of the yields from Fig. 3. The histogram is on a log scale to make the Σ^{*0} contribution visible.

histogram has a logarithmic scale to make the estimated yield visible.

The acceptance correction was performed using the simulation of non-resonant three-body phase space $K^+\Sigma^+\pi^-$. The generated and accepted events were binned in a four dimensional space of the independent kinematic variables, namely Q^2 (1.0 to 3.0 $(GeV/c)^2$), W (1.5 to 3.5 GeV), the missing mass of e^-K^+ , and cosine of the kaon angle in the center-of-mass frame of $K^+\Sigma^+\pi^-$. Another kinematic variable ϕ , which is the angle between the production plane characterized by K^+ and the scattering plane characterized by the scattered e^- , was not binned. This amounts to the assumption that σ_{LT} and σ_{TT} , the longitudinal-transverse and transverse-transverse interference structure functions, are small in this reaction. The dependence on this ϕ distribution was studied and the systematic uncertainties were obtained as follows. The phase-space generated Monte-

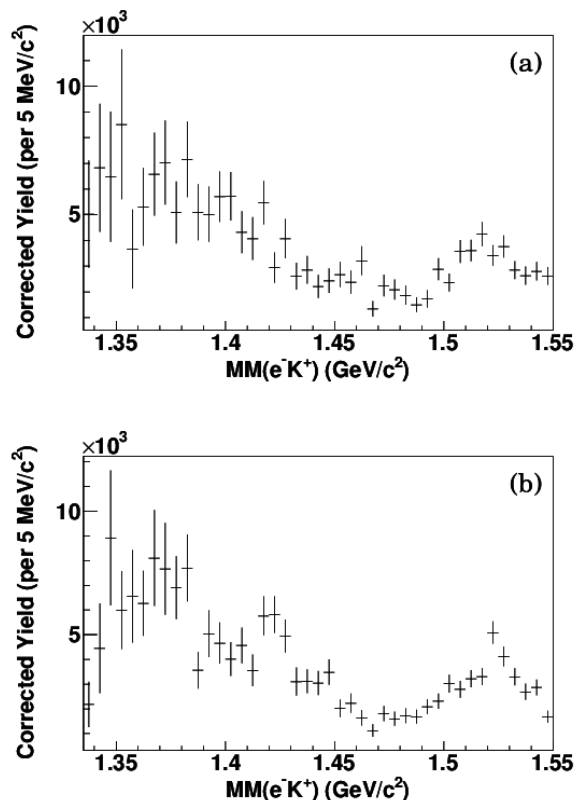


FIG. 6. Acceptance-corrected yield versus the missing mass of e^-K^+ for (a) $1.0 \leq Q^2 \leq 1.5$, and (b) $1.5 \leq Q^2 \leq 3.0$ $(GeV/c)^2$.

Carlo events already match the measured data distributions in Q^2 , W , and particle momenta well. Furthermore, an improved matching to data was achieved by selecting events in e^-K^+ missing mass and ϕ to tailor the Monte-Carlo distributions used in computing the acceptance. An acceptance factor was calculated bin by bin in order to reduce bin-averaging effects. The corrected hyperon yield is shown in Fig. 6, where Fig. 6(a) is for Q^2 from 1.0 to 1.5 $(GeV/c)^2$ and Fig. 6(b) for Q^2 from 1.5 to 3.0 $(GeV/c)^2$. The statistics in these two Q^2 regions are comparable. The rightmost peak in both figures is the $\Lambda(1520)$. A peak around 1.42 GeV/c^2 and another broader peak at the lower invariant mass in Fig. 6(b) are not consistent with the PDG values for the $\Lambda(1405)$ [1]. However, neither peak is seen clearly in the lower Q^2 range (Fig. 6(a)).

III. RESULTS

The higher Q^2 range distribution from Fig. 6(b) was fitted with the simulated background, the $\Lambda(1520)$ and various assumptions about the $\Lambda(1405)$. The results are shown in Fig. 7. The black points with error bars are the acceptance-corrected results. The shadowed histograms along the bottom show the estimated systematic uncer-

tainty in each mass bin. The systematic band was obtained by varying the selection of events (see Fig. 2), the acceptance distribution in ϕ , and the acceptance in the hyperon invariant mass line shape (missing mass of e^-K^+). Correlation between systematic uncertainties and statistical fluctuations happens very often in low-statistics experiments. This appears clearly in the lower invariant mass region. An empirical smoothing process to separate the fluctuations from the estimated systematic uncertainties was implemented. Quantitatively, the systematic uncertainties were obtained from the following three analysis variations.

1. The range of the event selection was narrowed to between 1.155 and 1.225 GeV/c^2 around the Σ^+ and to between 0.06 and 0.24 GeV/c^2 around the π^0 . The resulting variations in yields were smoothed by fitting the relative uncertainties to an empirical smoothing function in the lower invariant mass region. The resulting uncertainties were less correlated to the statistical fluctuation and closer to the pure systematic uncertainties. This contributed about 45% to the total bin-to-bin systematic uncertainty.
2. The phase-space Monte-Carlo distribution of events in ϕ matched the data fairly well. But an exact matching was enforced by accepting Monte-Carlo events selectively. A similar smoothing process was applied to the differences of acceptance-corrected yields between a uniform phase-space distribution and the matching distribution. The resulting differences contributed about 35% to the total systematic uncertainty.
3. The phase-space Monte-Carlo line shape of the hyperon invariant mass was modified to match exactly the observed line shape. The differences between the phase space distribution and the distribution that was closely matched to measured data were smoothed by averaging the neighboring bins. This systematic difference contributed about 20% to the total bin-to-bin systematic uncertainty.

The overall systematic bin-to-bin uncertainty shown in Fig. 7 was achieved by adding all pieces together in quadrature. The relative changes in strength between the observed peaks and the distortions of the peak shape due to radiative effects are small in comparison to the precision of these results. Hence radiative corrections were not performed.

In Fig. 7 the resonances are computed as incoherent relativistic Breit-Wigner functions of the form

$$BW(m) \approx \frac{1}{2\pi} \frac{4mm_0\Gamma(q)}{(m^2 - m_0^2)^2 + (m_0\Gamma(q))^2}. \quad (1)$$

In Eq. 1, $\Gamma(q) = \frac{q}{q_0}\Gamma_0$, m_0 , and Γ_0 are fit parameters, q is the momentum of π^- in the hyperon rest frame, and q_0 is value of the q when $m = m_0$.

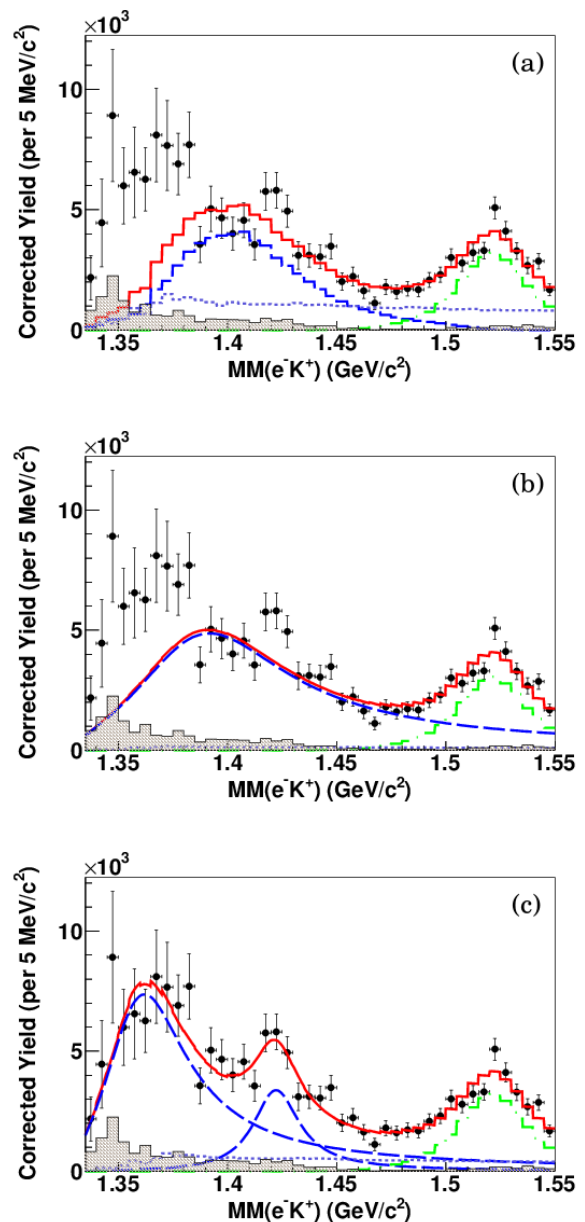


FIG. 7. (Color online) Fits of the missing mass of e^-K^+ for $1.5 < Q^2 < 3.0$ (GeV/c^2). Points with error bars are measured data, solid (red) lines are overall fits, dash-dotted (green) lines around $1.52 \text{ GeV}/c^2$ are from the $\Lambda(1520)$ simulation. The dashed (blue) lines are from the $\Lambda(1405)$ simulation parametrized by PDG values (a), by one relativistic Breit-Wigner function (b), and by two relativistic Breit-Wigner functions (c). The dotted (purple) lines show the summed background contributions. The shadowed histograms at the bottom show the estimated systematic uncertainty.

As seen in Fig. 7(a), a fit using a single Breit-Wigner line shape with PDG parameters gives a very poor representation of the data. The fit includes the summed background contribution, simulation of $\Lambda(1520)$ electroproduction, and simulation of a Breit-Wigner “resonance”

parametrized with the PDG values of the $\Lambda(1405)$. In Fig. 7(b), an alternative fit released these parameters from their PDG values. Also in this case, the freely-fitted Breit-Wigner is a poor fit to the data. In Fig. 7(c), we allowed the $\Lambda(1405)$ to be represented as two incoherent Breit-Wigner peaks. The best fit result gives the two peak positions at $m_0^{high} = 1.423 \pm 0.002$ GeV/ c^2 and $m_0^{low} = 1.368 \pm 0.004$ GeV/ c^2 , where the uncertainties include only the fit errors. This fit is clearly superior to the other two. The best-fit χ^2 per degree of freedom was 1.31 (Fig. 7(c)) compared to 3.12 (Fig. 7(a)) and 2.97 (Fig. 7(b)), respectively. A fit with two coherent Breit-Wigner line shapes was also tested, resulting in a χ^2 per degree of freedom 1.43, similar to the best fit and qualitatively the same.

Next, the acceptance-corrected yield was produced for seven Q^2 ranges, where the upper limit was fixed at 3.0 (GeV/ c)² and the lower limits were changed in steps from 1.0 to 2.2 (GeV/ c)², as shown in Fig. 8. Figure 8(a) shows the data for $1.0 \leq Q^2 \leq 3.0$ (GeV/ c)² and Fig. 8(g) for $2.2 \leq Q^2 \leq 3.0$ (GeV/ c)². The histograms were fitted with two relativistic incoherent Breit-Wigner functions, allowing only the amplitudes to vary from range to range, while the centroids and widths were common to all. This combined fit extracted the two peak positions $m_0^{high} = 1.422 \pm 0.002$ GeV/ c^2 , and $m_0^{low} = 1.365 \pm 0.002$ GeV/ c^2 , with a χ^2 per degree of freedom of 1.44. These values are consistent with the fit in Fig. 7(c), though we note that the error bars in this overall fit are correlated. It can be seen that the relative strength of the Breit-Wigner centered at m_0^{high} is increasing with increasing Q^2 compared to the one centered at m_0^{low} , while staying comparable in strength to the $\Lambda(1520)$. This variation in relative strength with increasing Q^2 is reminiscent of the expectation in chiral unitary models that coupling to the two poles should depend on the coupling to the initial state. However, no model has attacked the question of whether such a variation can be related to the Q^2 of a virtual photon.

The stability of these fits was tested by first adding and then subtracting the systematic uncertainty (shaded histograms) from the corrected yields. The fits were repeated on the modified yield distributions. The fit with two incoherent Breit-Wigner functions still showed the best result in terms of reduced χ^2 . This shows that the two-pole interpretation of our data remains the best, given the estimated systematic uncertainties.

IV. DISCUSSION AND CONCLUSIONS

The acceptance-corrected spectrum is qualitatively similar to an early result from a bubble chamber experiment by Braun *et al.* [24] for the reaction $K^-D \rightarrow \Sigma^- \pi^+ p$. Jido *et al.* [29] proposed the line shape as coming from interference of the $I = 1$ $\Sigma^*(1385)$ and an $I = 0$ pole at 1424 MeV/ c^2 . However, our electroproduction work measured the amount of $\Sigma^{*0}(1385)$ and found neg-

ligible contribution, as shown previously in Fig. 5. The expected yield of $\Sigma^{*0}(1385)$ is much smaller than the statistical fluctuation of the observed statistics. In addition, any interference between the $\Sigma^{*0}(1385)$ and the $\Lambda(1405)$ should vanish in this line shape. The reason is because the final line shape stems from integration over all decay angles. The $\Sigma^{*0}(1385)$ decays into $\Sigma\pi$ in P -wave, and the $\Lambda(1405)$ decays in S -wave. The distributions are orthogonal to each other and vanish after integrating over angles. Thus, we conclude that the whole of the measured background-subtracted distribution below the $\Lambda(1520)$ is due to the so-called $\Lambda(1405)$.

It has been shown in photoproduction (at $Q^2 = 0$) that the structure of the $\Lambda(1405)$ region is complex. Not only does the $N\bar{K}$ channel-coupling strongly distort the Breit-Wigner line shape used to represent the $\Lambda(1405)$, but there is also a significant $I = 1$ component to the reaction mechanism that is not coming from the $\Sigma^{*0}(1385)$ [17, 18]. With the limited statistical power of the present electroproduction data, it was not feasible to analyze these data in a similar framework. Higher statistics data would clearly be useful here.

We note that the best-fit masses found in this analysis, m_0^{low} and m_0^{high} , are close to a number of model predictions based on unitarized coupled channels models. Examples are the previously-quoted work of Jido *et al.* [10], and also Oller and Meißner [9], Ikeda *et al.* [12], [13], Guo and Oller [14], and Khemchandani *et al.* [16]. Agreement is less good with the work of Mai and Meissner [15] and the phenomenological photoproduction analysis of Schumacher and Moriya [18]. Again, higher statistics electroproduction data would clearly be useful.

To summarize, the $\Lambda(1405)$ mass region in electroproduction studied in this work is poorly described by a single Breit-Wigner distribution. Different fits have been tried and the best is with two relativistic Breit-Wigner functions, which supports the two-pole model as discussed in chiral unitary models [11]. In addition, the relative strength of two line shapes changes with Q^2 . The progression suggests that at higher Q^2 , which corresponds to more off-shell exchange kaons (see Fig. 1), it is more likely to excite the higher mass pole of the $\Lambda(1405)$ structure relative to the lower pole. The mass distribution seen in this measurement also differs markedly from what is seen in photoproduction at $Q^2 = 0$ [17, 18]. The present limited statistics makes more quantitative statements difficult, but the existence of this phenomenon has been established and encourages further exploration.

ACKNOWLEDGMENTS

We acknowledge the outstanding efforts of the staff of the Accelerator and Physics Divisions at Jefferson Lab that made this experiment possible. The work of the Medium Energy Physics group at Carnegie Mellon University was supported by DOE grant DE-FG02-87ER40315. The Southeastern Universities Research As-

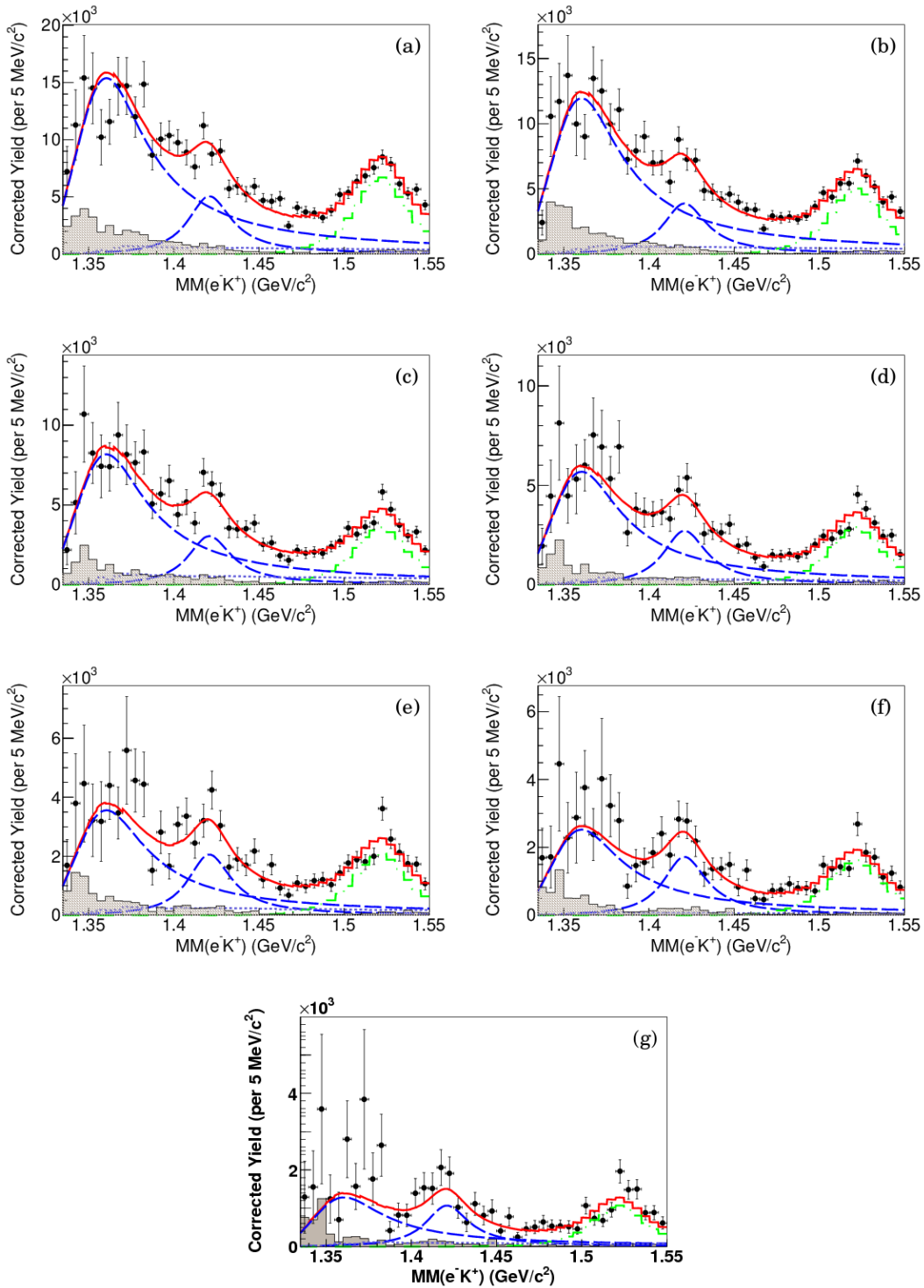


FIG. 8. (Color online) Overall fit of the acceptance-corrected missing mass of e^-K^+ with simulated background, simulated production of the $\Lambda(1520)$, and two relativistic Breit-Wigner functions in the ranges $Q_{min}^2 \leq Q^2 \leq 3.0$ (GeV/c)², where Q_{min}^2 is: (a) 1.0 (GeV/c)², (b) 1.2 (GeV/c)², (c) 1.4 (GeV/c)², (d) 1.6 (GeV/c)², (e) 1.8 (GeV/c)², (f) 2.0 (GeV/c)², and (g) 2.2 (GeV/c)². The fit takes the statistical uncertainties (error bars on points) into account. The shadowed histograms show the estimated systematic uncertainties.

sociation (SURA) operated the Thomas Jefferson National Accelerator Facility for the United States Department of Energy under contract DE-AC05-84ER40150. Support was also provided by the National Science Foun-

dation, the United Kingdom's Science and Technology Facilities Council (STFC), and the National Research Foundation of Korea.

-
- [1] J. Beringer *et al.* (Particle Data Group), Phys. Rev. **D86**, 010001 (2012).
- [2] R. H. Dalitz and S. F. Tuan, Phys. Rev. Lett. **2**, 425 (1959).
- [3] R. Dalitz and S. Tuan, Annals of Physics **10**, 307 (1960).
- [4] M. Alston *et al.*, Phys. Rev. Lett. **6**, 698 (1961).
- [5] N. Isgur and G. Karl, Physics Letters B **72**, 109 (1977).
- [6] N. Isgur and G. Karl, Phys. Rev. D **18**, 4187 (1978).
- [7] N. Isgur and G. Karl, Phys. Rev. D **19**, 2653 (1979).
- [8] S. Capstick and N. Isgur, Phys. Rev. D **34**, 2809 (1986).
- [9] J. Oller and U.-G. Meißner, Physics Letters B **500**, 263 (2001).
- [10] D. Jido, J. Oller, E. Oset, A. Ramos, and U.-G. Meißner, Nuclear Physics A **725**, 181 (2003).
- [11] T. Hyodo and D. Jido, Progress in Particle and Nuclear Physics **67**, 55 (2012).
- [12] Y. Ikeda, T. Hyodo, and W. Weise, Phys.Lett. **B706**, 63 (2011).
- [13] Y. Ikeda, T. Hyodo, and W. Weise, Nucl.Phys. **A881**, 98 (2012).
- [14] Z.-H. Guo and J. Oller, Phys.Rev. **C87**, 035202 (2013), arXiv:1210.3485 [hep-ph].
- [15] M. Mai and U.-G. Meißner, Nucl.Phys. **A900**, 51 (2013).
- [16] K. Khemchandani, A. Martinez Torres, H. Kaneko, H. Nagahiro, and A. Hosaka, Phys.Rev. **D84**, 094018 (2011).
- [17] K. Moriya, R. A. Schumacher, *et al.* (CLAS Collaboration), Phys. Rev. C **87**, 035206 (2013).
- [18] R. A. Schumacher and K. Moriya, Nucl. Phys. A (2013), 10.1016/j.nuclphysa.2013.03.003, (in press).
- [19] J. K. Ahn *et al.* (LEPS Collaboration), Nucl. Phys. **A721**, 715 (2003).
- [20] M. Niiyama *et al.* (LEPS Collaboration), Phys. Rev. **C78**, 035202 (2008).
- [21] G. Agakishiev *et al.* (HADES Collaboration), Phys.Rev. **C85**, 035203 (2012).
- [22] I. Zychor *et al.*, Phys. Lett. **B660**, 167 (2008).
- [23] R. J. Hemingway, Nucl. Phys. **B253**, 742 (1985).
- [24] O. Braun *et al.*, Nuclear Physics B **129**, 1 (1977).
- [25] D. W. Thomas, A. Engler, H. E. Fisk, and R. W. Kraemer, Nucl. Phys. **B56**, 15 (1973).
- [26] B. A. Mecking *et al.* (CLAS Collaboration), Nucl. Inst. and Meth. **503**, 513 (2003).
- [27] H. Y. Lu, R. A. Schumacher, B. Raue, and M. Gabrielyan (CLAS Collaboration), AIP Conf. Proc. **1432**, 199 (2012).
- [28] CERN_CN Division, "GEANT 3.2.1," CERN Program Library W5013 (1993).
- [29] D. Jido, E. Oset, and T. Sekihara, Eu. Phys. J. A **42**, 257 (2009).